Measurement of tunnel coupling in a Si double quantum dot based on charge sensing

Xinyu Zhao and Xuedong Hu*

Department of Physics, University at Buffalo, SUNY, Buffalo, New York 14260, USA

In Si quantum dots, valley degree of freedom, in particular the generally small valley splitting and the dot-dependent valley-orbit phase, adds complexities to the low-energy electron dynamics and the associated spin qubit manipulation. Here we propose a four-level model to extract tunnel coupling information for a Si double quantum dot (DQD). This scheme is based on a charge sensing measurement on the ground state as proposed in the widely used protocol for a GaAs double dot [DiCarlo et. al., PRL 92. 226801]. Our theory can help determine both intra- and inter-valley tunnel coupling with high accuracy, and is robust against system parameters such as valley splittings in the individual quantum dots.

INTRODUCTION

Tunnel coupling is an essential element in coherent manipulation of electron qubits in semiconductor quantum dots (QDs) [1–18]. It allows single-qubit operations on a charge qubit, and exchange gates for spin qubits [19–25]. Interdot shuttling is also crucial for information transfer on chip [26–33]. With spin and spin-charge hybrid qubits having been demonstrated as hopeful candidates for foundational building blocks of future quantum processors [34–40], accurately characterizing tunnel coupling between quantum dots is an imperative task in characterizing these qubits.

A robust approach to detect tunnel coupling in a DQD was developed more than a decade ago [41] based on measuring the charge distribution of the DQD in thermal equilibrium as a function of the interdot detuning, then fits a two-level (2L) model [42] to obtain the tunnel coupling between the two single-dot ground states. This measurement technique is particularly successful for a GaAs DQD, where excited orbital states are generally several meV above the ground state while experimental temperature is kept at about 100 mK (for a thermal energy of $\sim 10\mu$eV), so that the 2L model including only the single-dot ground states works perfectly [41, 43].

In recent years, studies of spin qubits have focused on Si QDs because of their superior coherence properties [34–40, 44]. The thermal equilibrium charge sensing technique has been widely used to measure tunnel coupling between the ground orbital states of two neighboring dots [45–53]. However, in Si-based QDs, the valley degree of freedom introduces extra energy levels a fraction of meV above the ground states, making the Si DQDs better described as a four-level (4L) system instead of a 2L system. There are also two relevant tunnel coupling parameters instead of one. Clearly, a 2L model cannot represent all the relevant properties of a Si DQD. It is not even clear whether it is capable of consistently producing accurate measurement of the ground state tunnel coupling. Although alternative schemes such as spin-cavity coupling
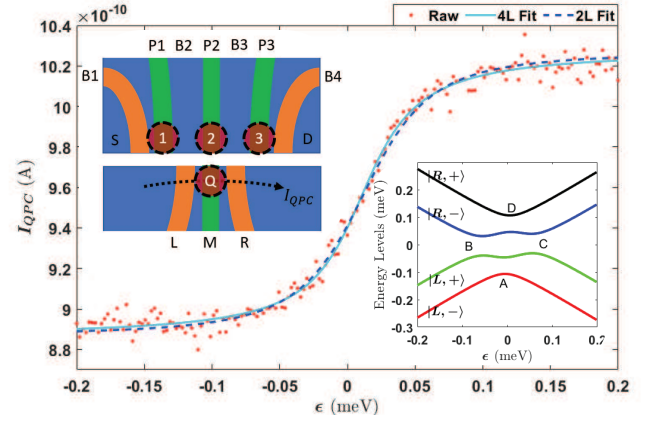

Figure 1. The $I_{QPC}(\epsilon)$ curve measured form experiment (red-doted markers) and the best fit curves. top-left inset: Schematic diagram of triple dot configuration. QDs "1,2,3" are confined under the plunger gates "P1, P2, P3". Dot "1-2" and "2-3" forms two DQD systems. Barrier gates "B1" to "B4" control the tunneling strength. Dot "Q" plays the role of charge sensor. Bottom-right inset: Typical energy levels of DQD.

have been employed to successfully measure tunnel coupling [54], the thermal equilibrium charge sensing technique will still be the most easily accessible and widely used in the foreseeable future. As such, it is important to develop an updated procedure of measuring tunnel coupling in a Si DQD that accounts for the valley dynamics.

In this paper, we develop a four-level (4L) model for the thermal equilibrium charge sensing measurement of tunnel coupling for a Si DQD. Specifically, we develop a numerical 4L fitting procedure for both intra- and inter-valley tunnel couplings of a Si DQD. We also derive a perturbative 4L fitting formula, which speeds up the fitting procedure dramatically while maintaining high degree of accuracy under most conditions. We apply the updated fitting procedures on multiple sets of data obtained in a linear Si/SiGe triple quantum dot (schematic diagram in Fig. 1) provided by Adam Mills and Jason Petta [4, 47], and produce consistent fitting for sometimes noisy experimental data. We compare the results from these new fitting procedures with the conventional

* xhu@buffalo.edu

2L-based approach, and find significant differences under common conditions. For example, in a particular DQD, we observe an average of 46% difference in the intra-valley tunnel coupling between the 2L fitting and 4L fitting. For a particular set of data, the two models make totally contradictory predictions on tunnel couplings, with the 4L prediction more consistent with the experimental procedure. These examples clearly illustrate the advantages and necessity of the 4L model in obtaining a reliable estimate of tunnel coupling in a Si DQD. Lastly, we analyze the robustness of our fitting procedure and identify possible errors.

RESULTS

Charge distribution in a four-level model

The six-fold degeneracy of the Si conduction band is lifted by the growth-direction (nominally the z direction) confinement near an interface, which leaves two of the bulk valleys with lower energy, denoted as $|z\rangle$ and $|\bar{z}\rangle$ states. Scattering at the interface further couples $|z\rangle$ and $|\bar{z}\rangle$ states [15, 16, 55], leading to the valley eigenstates $|\pm\rangle = \frac{1}{\sqrt{2}} \left(|z\rangle \pm e^{i\phi}|\bar{z}\rangle \right)$, where the phase ϕ is determined by the interface scattering matrix element. The energy splitting $2|\Delta|$ between $|\pm\rangle$ states is called the valley splitting, and is typically 0.1 to 0.2 meV in a SiMOS quantum dot and $\lesssim 0.1$ meV in a Si/SiGe dot. Compared to the few meV orbital excitation energy in these quantum dots due to in-plane confinement, valley splitting is much smaller, making it reasonable to neglect intra-valley orbital excitation but include both valleys when considering charge distribution in thermal equilibrium at low temperatures.

A minimal model for the low-energy single-electron charge distribution and dynamics of a Si DQD should thus include the ground orbital state in each dot (denoted as $|L\rangle$ and $|R\rangle$ for left and right dot), together with both valley eigenstates, leading to four basis states: $\{|L,+\rangle, |L,-\rangle, |R,+\rangle,$ and $|R,-\rangle\}$. Considering that interdot barrier is generally a smooth variation in electrical potential at a length scale much larger than the lattice constant, tunneling is only allowed between states in the same bulk valley: $\langle L,z|H|R,z\rangle = t_C$ is finite while $\langle L,z|H|R,\bar{z}\rangle = 0$. Using the four basis states $|D,\pm\rangle = \frac{1}{\sqrt{2}}(|D,z\rangle \pm e^{i\phi_D}|D,\bar{z}\rangle)$ $(D = L, R)$ with local phases ϕ_D, the single-electron Hamiltonian in the Si DQD can be expressed as

$$H = \begin{bmatrix} \epsilon + |\Delta_L| & 0 & t_+ & t_- \\ 0 & \epsilon - |\Delta_L| & t_- & t_+ \\ t_+^* & t_-^* & -\epsilon + |\Delta_R| & 0 \\ t_-^* & t_+^* & 0 & -\epsilon - |\Delta_R| \end{bmatrix}. \tag{1}$$

Here ϵ is the interdot detuning, $|\Delta_{L,R}|$ are the L/R valley splittings, $t_\pm = \frac{1}{2}t_C[1 \pm e^{-i\delta\phi}]$ are the intra- and inter-valley (here "valley" means the valley eigenstates $|\pm\rangle$) tunnel couplings, respectively, and $\delta\phi = \phi_L - \phi_R$ is the valley phase difference between the two dots.

Hamiltonian (1) can be numerically diagonalized at any given detuning ϵ to obtain the eigenvalues E_i and the corresponding eigenstates $|\Psi_i\rangle$ ($i = 1, 2, 3, 4$). It can also be diagonalized analytically, though the general expressions are cumbersome and not transparent. If we treat inter-valley tunneling as a perturbation, on the other hand, we can obtain simple analytical expressions for E_i and $|\Psi_i\rangle$, (see the "Methods" section), which can be used in a fitting procedure much more conveniently. Specifically, the left-dot charge distribution for each eigenstate $|\Psi_i\rangle$ takes the form

$$P_{L1} = \cos^2 \frac{\Theta_1}{2} \sin^2 \frac{\theta_-}{2} + \sin^2 \frac{\Theta_1}{2} \cos^2 \frac{\theta_+}{2},$$

$$P_{L2} = \sin^2 \frac{\Theta_2}{2} \cos^2 \frac{\theta_-}{2} + \cos^2 \frac{\Theta_2}{2} \sin^2 \frac{\theta_+}{2},$$

$$P_{L3} = \cos^2 \frac{\Theta_2}{2} \cos^2 \frac{\theta_-}{2} + \sin^2 \frac{\Theta_2}{2} \sin^2 \frac{\theta_+}{2},$$

$$P_{L4} = \sin^2 \frac{\Theta_1}{2} \sin^2 \frac{\theta_-}{2} + \cos^2 \frac{\Theta_1}{2} \cos^2 \frac{\theta_+}{2}. \tag{2}$$

Here $\tan\Theta_1 = \frac{|t_-|}{E_+ + E_- + \Delta_+}$, $\tan\Theta_2 = \frac{|t_-|}{E_+ + E_- - \Delta_+}$, and $\tan\theta_\pm = \frac{|t_+|}{\epsilon \pm \Delta_-}$ ($\theta_\pm \in [0,\pi]$), with $E_\pm = \sqrt{(\epsilon \pm \Delta_-)^2 + |t_+|^2}$ and $\Delta_\pm = \frac{1}{2}(|\Delta_L| \pm |\Delta_R|)$. The expressions given in Eq. (2) become exact if $|\Delta_L| = |\Delta_R|$. A more detailed study in the "Methods" section shows that the approximation underlying Eq. (2) is valid in most regions of the parameter space. For example, there is only a 4% error when $|\Delta_L|$ and $|\Delta_R|$ are different by 20%.

When the single electron in the DQD is in thermal equilibrium, its density matrix is given by a thermal state $\rho = \sum_i \frac{1}{Z} e^{-\beta E_i} |\Psi_i\rangle\langle\Psi_i|$, where $\beta = \frac{1}{k_B T}$, k_B is the Boltzmann constant, and $Z = \sum_i e^{-\beta E_i}$ is the partition function. The total charge occupation in the left dot at temperature T is then

$$P_L = \sum_i \frac{1}{Z} e^{-\beta E_i} P_{Li}. \tag{3}$$

Here P_L is a function of both tunnel couplings $t_\pm$, both valley splittings $|\Delta_L|$ and $|\Delta_R|$ (with their phase difference $\delta\phi$ already contained in $t_\pm$), and detuning ϵ. Given experimentally measured $P_L(\epsilon)$, we could thus obtain $t_\pm$ via data fitting. In theory one could obtain the valley splittings from this fitting procedure as well, though our numerical studies below show that the results are not particularly sensitive to $|\Delta_{L,R}|$, making the information obtained from fitting less reliable. Thus we generally treat valley splittings as known parameters.

There are two major reasons that cause different predictions between 2L and 4L theories. First, the different number of levels involved means that the thermal occupations are distributed differently. The impact of this thermal occupation is typically limited since experimental temperature is usually about 100 mK and much smaller

than valley splittings in the dots. Obvious exceptions include cases when the valley splittings are very small (for example $\sim 10\mu\text{eV}$, similar to the thermal energy), or when the temperature is much higher than usual. Second, and more importantly, all eigenstates $|\Psi_i\rangle$ in a Si DQD contain the valley excited states $|+\rangle$ due to the finite inter-valley tunnel coupling. The involvement of the excited valley states causes subtle changes to the state compositions, which then lead to differences in the charge distribution.

In the absence of inter-valley tunneling ($\delta\phi = 0$), the two valley eigenstates decouple into their own subspaces, so that the charge distribution is reduced to an exact analogy to the two-level case in GaAs when we neglect the thermal occupation of the excited valley states

$$P_L = \frac{1}{2}\left[1 - \frac{\epsilon - \Delta_-}{2E_+}\tanh\left(\frac{E_+}{2k_B T}\right)\right]. \qquad (4)$$

This is just the fitting formula in Ref. 41 with an ϵ shift caused by asymmetric valley splittings. If we impose a further condition that the valley splittings are symmetric ($\Delta_- = 0$), the thermal occupation of the excited valley states would have the same left-right distribution as the ground valley states, so that the 4L theory we develop here would become identical to the conventional 2L model. In other words, under the condition

$$\delta\phi = 0 \quad \& \quad |\Delta_L| = |\Delta_R| \qquad (5)$$

Eq. (2) and Eq. (3) would lead exactly to the 2L fitting formula in Ref. 41, as is Eq. (4).

Extracting tunnel couplings from charge distributions

The functional forms for charge distribution in a Si DQD given by Eqs. (2) and (3) allow us to obtain tunnel couplings $t_\pm$ (or t_C and $\delta\phi$) between the two dots by fitting experimentally measured $P_L(\epsilon)$, similar to the procedure given in Ref. 41.

As we discussed above, the charge distribution P_L is a function of multiple parameters and variables: $P_L = P_L(\Delta_L, \Delta_R, t_+, t_-, \epsilon)$. To obtain more constrained and reliable knowledge of the tunnel couplings, the valley splittings Δ_L and Δ_R should be known beforehand, for example through the spin relaxation hot spot for each dot [56]. If $|\Delta_{L,R}|$ are not known a priori, one can use an estimate instead, without creating significant errors. A detailed discussion of the consequences of not knowing these splittings is given in the "Methods" section.

Experimentally, what is measured is the charge sensor (for example a quantum point contact, or QPC) current as a function of the interdot detuning: $I_{QPC}(\epsilon)$. The current is usually assumed to be linearly related to the charge distribution in the DQD [41]:

$$I_{QPC} = I_0 + \delta I \cdot P_L(\epsilon) + \delta I_{noise}, \qquad (6)$$

where I_0 is the background current (setting a reference point), δI is the linear conversion ratio, and δI_{noise} is the noise in the I_{QPC} measurement. The first two parameters are part of the fitting procedure and the impact of δI_{noise} will be discussed in the "Methods" section. In addition, the inter-dot detuning may also have a background voltage, i.e., $\epsilon_m = \epsilon_0 + \epsilon$, where ϵ_m is the value measured in the experiment and ϵ_0 is a reference shift.

Our fitting procedure thus consists of the following steps. First we use Eq. (3) or Eq. (4) (for 4L or 2L fitting respectively) to generate a theoretical curve $I_{th}(\epsilon)$ with a set of candidate fitting parameters such as $t_\pm$. We then calculate the deviation from the experimental data, and minimize it by varying the fitting parameters. While the three parameters I_0, δI, and ϵ_0 are part of the fitting parameter set, they take up different roles compared to $t_\pm$. The tunnel couplings $t_\pm$ determine the "shape" of the curve, while these three parameters determine the positions of the curve. In particular, ϵ_0 determines the shift in the horizontal (detuning) direction, I_0 determines the vertical shift, while δI is a scaling factor. None of them contributes to the shape or curvature of the curve near $\epsilon = 0$, which is determined by $t_\pm$. Therefore, they can be obtained separately from the main fitting parameters $t_\pm$. One can follow an adaptive fitting procedure that fit these two groups of parameters in turn until they converge to steady values, respectively. A discussion about the fitting inaccuracy caused by errors in $I_0, \delta I$, and ϵ_0 can be found in the "Methods" section, particularly in Fig. 7.

Fitting actual experimental data: an example

With the procedure described above, we examine some experimental data acquired during the tune-up of a linear array of 9 QDs used to demonstrate charge shuttling [4, 33, 47]. The measurements were performed on a triple dot schematically shown in Fig. 1. It is part of a Si/SiGe 9-dot array with three QPCs as charge sensors [4, 33, 47]. The experimental temperature is at $T = 50$ mK [47] and the valley splittings $|\Delta_L|$ and $|\Delta_R|$ are estimated to be around 66-74 μeV from spin measurements in the same device [57]. For each DQD, the $I_{QPC}(\epsilon)$ curve are measured with four different barrier gate voltage V_{B2} (or V_{B3}). One set of data, together with our fitting curve, is shown in Fig. 1. All other data sets and fitting curves are shown in Fig. 4 in the "Methods" section.

The tunnel couplings and other parameters we obtained from data fitting are summarized in Table I. In particular, the inter-dot valley phase difference $\delta\phi$ for QD 1-2 in Table I is roughly a constant under different applied V_{B2}, which implies that varying V_{B2} only changes the interdot barrier height, but does not cause the dots to shift to any significant degree. Consequently, in the 4L model only t_C depends on V_{B2}, while $\delta\phi$ does not.

The tunnel couplings are obtained with different fitting formulas: (A). Eq. (4), labeled as "2L", (B). Eq. (3)

QD 1-2	(a)	(b)	(c)	(d)
2L $|t_+|$	24 ± 0.6	43 ± 1.1	53 ± 1.0	70 ± 2.5
4L $|t_+|$ (N.)	20 ± 1.2	32 ± 1.9	37 ± 2.6	37 ± 6.0
4L $|t_+|$ (F.)	20 ± 1.1	33 ± 1.8	37 ± 2.6	38 ± 5.7
4L $|t_-|$	39 ± 4.7	64 ± 4.8	76 ± 5.9	112 ± 12
4L $\delta\phi$ (rad)	2.2 ± 0.05	2.2 ± 0.03	2.2 ± 0.04	2.5 ± 0.06
QD 2-3	(e)	(f)	(g)	(h)
2L $|t_+|$	22 ± 0.6	41 ± 0.8	44 ± 0.8	$\mathbf{36} \pm 1.3$
4L $|t_+|$ (N.)	22 ± 0.7	41 ± 1.7	44 ± 1.6	26 ± 2.5
4L $|t_+|$ (F.)	22 ± 0.8	41 ± 1.6	44 ± 1.6	26 ± 2.5
4L $|t_-|$	0 ± 9.6	0 ± 14	0 ± 14	62 ± 7.1
4L $\delta\phi$ (rad)	0 ± 0.22	0 ± 0.20	0 ± 0.18	2.3 ± 0.04

Table I. Best fitting parameters for tunnel couplings. Data set (a)-(d) are measured from dot 1-2 and fitted with $|\Delta_L| = 66$ μeV, $|\Delta_R| = 74$ μeV. Data set (e)-(h) are measured from dot 2-3 and fitted with $|\Delta_L| = 74$ μeV, $|\Delta_R| = 74$ μeV. $|t_\pm|$ units are μeV. (N.) means using numerical diagonalization, (F.) means using Eq. (2).

and (2), labeled as "4L (F.)", (C). Eq. (3), with a numerical diagonalization of H to calculate P_{Li}, labeled as "4L (N.)". According to the fitting results, the analytical formula Eq. (2) provides almost the same results as numerically diagonalizing the Hamiltonian. The average difference between 4L $|t_+|$ (F.) and 4L $|t_+|$ (N.) is only **0.9%**, which indicates that Eq. (2) is very accurate here. Additional discussion about the accuracy of Eq. (2) will be presented in following subsections as well as in the "Methods" section.

In comparison, the 2L fitting results are quite different from the 4L results: the average difference between 2L $|t_+|$ and 4L $|t_+|$ for QD 1-2 is **46%** across the different barrier heights in Table I, with 2L model consistently producing larger tunnel splittings. Qualitatively, this deviation is due to the fact that in the 2L model we are using a single excited level to represent the effect of three excited levels in the 4L model. As such this single excited state needs to be above the first excited state but lower than the third excited state in the 4L model, so that $|t_+|$ in the 2L model has to be larger than that in the 4L model. The error bars are obtained by numerically generating various stochastic realization of δI_{noise} with the same standard deviation as the measured data and then fitting all realizations. Here we assume the uncertainty mainly comes from the noise in the I_{QPC} signal as shown in Fig. 1, which is the conclusion from Ref. [41] as well.

We perform the curve fitting with several combinations of $|\Delta_L|$ and $|\Delta_R|$ within the estimated range of 66 to 74 μeV. The parameters presented in Table I are chosen because they produce the most consistent fitting results for $\delta\phi$. The fitting results for other $|\Delta_{L,R}|$ are shown in Fig. 5 in the "Methods" section.

The best fittings for QD 2-3 are shown in Table I, data set (e)-(h). A notable contradiction arises for (h). The 2L theory predicts $t_C = |t_+| = 36\mu$eV for (h), which is smaller than $t_C = |t_+| = 44\mu$eV for (g), even though the

increase in V_{B3} from (g) to (h) should cause the barrier height to decrease and tunnel coupling to increase [57]. This abnormality does not show up in the 4L theory, which suggests that $t_C = \sqrt{|t_+|^2 + |t_-|^2} = 67\mu$eV for (h), larger than $t_C = 44\mu$eV for (g). However, the 4L result of $\delta\phi$ for (h) is remarkably different from other fitting results for QD 2-3, as if the dots have shifted so that at least one of the dots has a significantly different valley phase. Indeed multiple factors could cause this change in $\delta\phi$. A physical reason such as possible interface steps in the DQD [58] could lead to such a shift. Other reasons, such as the relatively noisy data (see Fig. 4 in the "Methods" section) or non-linear effect in Eq. (6) [41], could cause a change in $\delta\phi$, too. Under imperfect conditions, such as a large δI_{noise} for (h), both 2L and 4L theory may fail to provide accurate fitting results, although the 2L prediction is qualitatively worse since it contradicts the experimental procedure.

The example given in Fig. 1 and Table I clearly shows that our 4L model is a much better representation of a Si DQD, and provides more reliable knowledge of the tunnel coupling in the DQD compared to the 2L model that has been widely used so far. Qualitatively, the 2L theory only includes the intra-valley tunneling reflected by anti-crossing "A" in Fig. 1, resulting in a simple form of ground state charge distribution $P_L = \sin^2 \frac{\theta_-}{2}$. The inter-valley tunneling reflected by anti-crossings "B" and "C" are taken into account in our 4L theory. They provide a correction to the 2L theory as represented by the factors $\cos^2 \frac{\Theta_1}{2}$ and $\sin^2 \frac{\Theta_1}{2}$ (t_- dependent) in Eq. (2). The details are presented in the "Methods" section and the magnitude of the 4L corrections from "B" and "C" will be discussed further in the next subsection.

Comparison between two-level and four-level models

Our results above show that 2L fitting returns quite different numbers from the 4L fitting. Nevertheless, it is still valuable to investigate the differences between the two models in a wide range of experimental conditions (under various $|t_\pm|$, $|\Delta_{L,R}|$, T, etc.), to better clarify their applicability in experimental studies of Si DQDs, which is the subject of this subsection.

In order to investigate a certain set of parameters ($|t_\pm|$, $|\Delta_{L,R}|$, T) other than the measured ones shown in Table I, we employ the Hamiltonian (1) to calculate a "pseudo-curve" $I_{QPC}(\epsilon)$ theoretically with given parameters. It represents an expected $I_{QPC}(\epsilon)$ curve measured in experiments with particular parameters. Then, we apply the procedure we proposed to fit this "pseudo-curve" and compare the fitted parameters with the original parameters used to generate the curve.

We first discuss qualitatively the necessary condition for a 4L model description of a Si DQD. Consider two well separated dots, when $t_\pm$ can be treated as perturbations in Eq. (1). The eigen-states $|\Psi_i\rangle$ are mainly the four unperturbed states $|L, \pm\rangle$, $|R, \pm\rangle$ except near
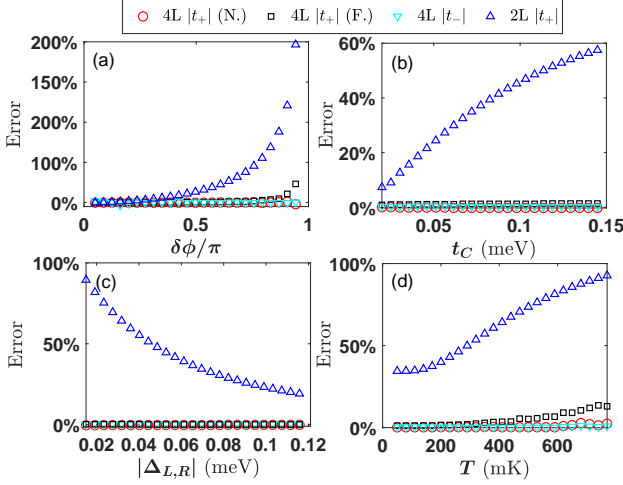
Figure 2. Errors for different fitting methods. The parameters to generate the "pseudo-curve" are $|\Delta_L| = 0.066$ meV, $|\Delta_R| = 0.074$ meV. $t_C = 0.071$ meV, $\delta\phi = 0.7\pi$, and $T = 50$ mK unless specified explicitly in the figures. As shown in the legend, the blue-upper-triangles are results from the 2L formula (4), the red circles are obtained via numerical diagonalization of the 4L Hamiltonian, while the black squares are from the 4L analytical formula of Eq. (2).

the anti-crossings. For example, when ϵ is in the region $\epsilon_A \pm \Delta\epsilon$, where $\epsilon_A = (|\Delta_L| - |\Delta_R|)/2$ is the center of anti-crossing "A", the ground state would be a mixture of $|L, -\rangle$ and $|R, -\rangle$. The range of this "mixing region" is roughly in the order of intra-valley tunneling, $\Delta\epsilon \sim |t_+|$. Outside the "mixing region", eigen-states $|\Psi_i\rangle$ are not affected by the this anti-crossing and remain the unperturbed states. Similarly, anti-crossings "B" and "C" also have their own "mixing regions", but mix different states $|L, +\rangle \to |R, -\rangle$ or $|L, -\rangle \to |R, +\rangle$, with a different magnitude of $\Delta\epsilon \sim |t_-|$. The charge distribution of the ground state is mainly determined by anti-crossing "A", as illustrated in Fig. 1. The impacts of "B" and "C" can be regarded as corrections. Therefore, when "B" and "C" are far away from "A", the impacts are limited and the dynamics is roughly a 2L dynamics with a single anti-crossing "A". In other words, under the condition

$$|\epsilon_A - \epsilon_B| = |\Delta_L| \gg |t_-| \quad \& \quad |\epsilon_A - \epsilon_C| = |\Delta_R| \gg |t_-|, \tag{7}$$

the 2L theory proposed in Ref. 41 is still a good approximation to describe the ground state charge distribution of a Si DQD. When the condition (7) is not fulfilled, on the other hand, a 4L model is necessary.

In Fig. 2 we provide numerical evidences for the condition (7), in the form of fitting errors' dependences on various system parameters. Specifically, Fig. 2(a) shows the effects of $\delta\phi$ with a fixed t_C and valley splittings. Clearly, Eq. (7) is fulfilled when $|t_-| \approx 0$, which requires $\delta\phi \approx 0$. In this case, the valley states $|+\rangle$ does not couple to $|-\rangle$, and the 4L system is approximately reduced to a pair of 2L system. When $\delta\phi$ is finite, on the other

hand, the 2L fitting generally results in significant errors, especially when $\delta\phi \to \pi$. At this limit $|t_+| \to 0$, making the 2L model unstable and sensitive to any data noise.

Figure 2 (b), (c), and (d) show the effects of tunnel coupling t_C, valley splittings $|\Delta_L|$ and $|\Delta_R|$, and temperature. The results are all consistent with condition Eq. (7). Here t_C represents tunnel coupling between bulk valleys, and is not directly measurable. However, larger t_C leads to larger $|t_-|$ for a given $\delta\phi$, making the 2L theory less reliable as the condition Eq. (7) is weakened. Similarly, when $|\Delta_{L,R}|$ is large, the fitting error by 2-level theory is significantly suppressed, while a smaller $|\Delta_{L,R}|$ leads to overlapping of mixing regions for anti-crossings A, B, and C, and the 2-level theory fails. The large errors of the 2L fitting at higher temperatures are also expected, as there is only one excited state with a simple ϵ dependence as opposed to three excited states with much more complex ϵ dependence.

One advantage of the 4L theory is that it automatically extracts inter-valley tunnel coupling t_- from the ground state charge distribution, as shown with the cyan triangles in all four subplots of Fig. 2. We also note that the approximate charge distributions given by the analytical expressions in Eq. (2) is very accurate except in a very small region when $\delta\phi \approx \pi$ in Fig. 2 (a). Therefore, Eq. (2) are a perfect approximation in most cases, allowing a much faster fitting calculation compared to a fully numerical procedure. A more detailed study on the accuracy of Eq. (2) is in the "Methods" section and Fig. 3.

There are also other practical factors affecting the accuracy of the fitting such as the inaccurate fitting of the parameters δI, I_0, ϵ_0, insufficient information of $|\Delta_{L,R}|$, and signal noise in I_{QPC}. The impacts of all these factors are discussed in the "Methods" section.

DISCUSSION

In this paper, we present a four-level model that can extract tunnel coupling information in a Si double quantum dot via measurement of charge distribution of the double dot in thermal equilibrium. In essence, we have adapted the protocol originally proposed and used for GaAs double dot [41] to a Si DQD by including the valley-orbit coupling and dynamics. We demonstrate the efficiency and robustness of our model and the associated fitting procedure by applying it to experimental data collected in a pair of Si DQD $I_{QPC}(\epsilon)$ [47]. The results clearly demonstrate the superiority of the 4L model compared to the conventional two-level model used in the original proposal, with the 2L model produces almost 50% larger tunnel coupling t_+, not to mention that only by the 4L model can one extract any information on the inter-valley tunnel coupling t_-. In addition to directly diagonalizing the 4L model Hamiltonian in the fitting procedure, we have also derived a set of approximate formula with the assumption that t_- can be treated

perturbatively. Our numerical results show that the approximate formula perform nearly perfectly in the vast majority of parameter regimes, with the only exception near the point where the inter-dot valley phase difference is π. Lastly, we compare the performance of the 2L and 4L models, and clarify the condition under which 4L model is necessary. In short, our 4L model for a Si DQD provides much better accuracy in extracting the intravalley tunnel coupling t_+ from a charge distribution measurement, while carrying the extra benefit of also extracting inter-valley tunnel coupling t_-. We hope that the proposed protocol can help experimentalists to measure tunnel couplings for a Si DQD more accurately and efficiently.

METHODS

Theoretical charge distribution

In our approximate treatment, we consider inter-valley tunnel coupling as a perturbation, while include intra-valley tunnel couplings in the unperturbed Hamiltonian. In essence we take a DQD with a completely smooth interface as our starting point. The Hamiltonian (1) can thus be split into two parts

$$H = H_0 + H_1, \tag{8}$$

where

$$H_0 = \begin{bmatrix} \epsilon + |\Delta_L| & 0 & t_+ & 0 \\ 0 & \epsilon - |\Delta_L| & 0 & t_+ \\ t_+^* & 0 & -\epsilon + |\Delta_R| & 0 \\ 0 & t_+^* & 0 & -\epsilon - |\Delta_R| \end{bmatrix}, \tag{9}$$

$$H_1 = \begin{bmatrix} 0 & 0 & 0 & t_- \\ 0 & 0 & t_- & 0 \\ 0 & t_-^* & 0 & 0 \\ t_-^* & 0 & 0 & 0 \end{bmatrix}. \tag{10}$$

The eigen-energies and eigen-states of H_0 are

$$E_{1,\pm} = \pm\Delta_+ - E_\pm \tag{11}$$

$$E_{2,\pm} = \pm\Delta_+ + E_\pm \tag{12}$$

where $E_\pm = \sqrt{(\epsilon \pm \Delta_-)^2 + |t_+|^2}$ and $\Delta_\pm = \frac{1}{2}(|\Delta_L| \pm |\Delta_R|)$, and the corresponding eigen vectors are

$$|\psi_{1,\mp}\rangle = \cos\frac{\theta_\mp}{2}|R,\mp\rangle - e^{-i\delta\phi/2}\sin\frac{\theta_\mp}{2}|L,\mp\rangle \tag{13}$$

$$|\psi_{2,\mp}\rangle = e^{i\delta\phi/2}\sin\frac{\theta_\mp}{2}|R,\mp\rangle + \cos\frac{\theta_\mp}{2}|L,\mp\rangle \tag{14}$$

where $\tan\theta_\mp = \frac{|t_+|}{\epsilon\mp\Delta_-}$ ($\theta_\mp \in [0,\pi]$).

When the inter-valley tunneling $|t_-|$ is finite, the Hamiltonian H can be rewritten in the new basis $\{|\psi_{1,\mp}\rangle, |\psi_{2,\mp}\rangle\}$. The matrix representation of H_0 becomes diagonal and the matrix elements of H_1 can be obtained as, for example,

$$\langle\psi_{1,-}|H_1|\psi_{1,+}\rangle = -i|t_-|\sin\left(\frac{\theta_-}{2} - \frac{\theta_+}{2}\right) \tag{15}$$

$$\langle\psi_{1,-}|H_1|\psi_{2,+}\rangle = t_-^*\cos\left(\frac{\theta_-}{2} - \frac{\theta_+}{2}\right) \tag{16}$$

When $|\Delta_L| = |\Delta_R|$, $\theta_- = \theta_+$. As a result, $\cos\left(\frac{\theta_-}{2} - \frac{\theta_+}{2}\right) = 1$ and $\sin\left(\frac{\theta_-}{2} - \frac{\theta_+}{2}\right) = 0$. In the new basis $\{|\psi_{1,\mp}\rangle, |\psi_{2,\mp}\rangle\}$, the rotated full Hamiltonian $\tilde{H}$ can be written as

$$\tilde{H} = \begin{bmatrix} -\Delta_+ - E_- & 0 & 0 & t_-^* \\ 0 & -\Delta_+ + E_- & t_-^* & 0 \\ 0 & t_- & \Delta_+ - E_+ & 0 \\ t_- & 0 & 0 & \Delta_+ + E_+ \end{bmatrix} \tag{17}$$

The eigen-energies are then

$$E_1 = \frac{1}{2}\left(E_+ - E_- - \sqrt{(E_+ + E_- + 2|\Delta_+|)^2 + |t_-|^2}\right) \tag{18}$$

$$E_2 = \frac{1}{2}\left(E_- - E_+ - \sqrt{(E_+ + E_- - 2|\Delta_+|)^2 + |t_-|^2}\right) \tag{19}$$

$$E_3 = \frac{1}{2}\left(E_- - E_+ + \sqrt{(E_+ + E_- - 2|\Delta_+|)^2 + |t_-|^2}\right) \tag{20}$$

$$E_4 = \frac{1}{2}\left(E_+ - E_- + \sqrt{(E_+ + E_- + 2|\Delta_+|)^2 + |t_-|^2}\right) \tag{21}$$

and the corresponding eigen-states are

$$|\Psi_1\rangle = e^{i\phi}\cos\frac{\Theta_1}{2}|\psi_{1,-}\rangle - \sin\frac{\Theta_1}{2}|\psi_{2,+}\rangle \tag{22}$$

$$|\Psi_2\rangle = -e^{i\phi}\sin\frac{\Theta_2}{2}|\psi_{2,-}\rangle + \cos\frac{\Theta_2}{2}|\psi_{1,+}\rangle \tag{23}$$

$$|\Psi_3\rangle = e^{i\phi}\cos\frac{\Theta_2}{2}|\psi_{2,-}\rangle + \sin\frac{\Theta_2}{2}|\psi_{1,+}\rangle \tag{24}$$

$$|\Psi_4\rangle = e^{i\phi}\sin\frac{\Theta_1}{2}|\psi_{1,-}\rangle + \cos\frac{\Theta_1}{2}|\psi_{2,+}\rangle \tag{25}$$

where $\tan\Theta_1 = \frac{|t_-|}{E_+ + E_- + \Delta_+}$ and $\tan\Theta_2 = \frac{|t_-|}{E_+ + E_- - \Delta_+}$. The left-dot charge distribution $|\langle L,-|\Psi_i\rangle|^2 + |\langle L,+|\Psi_i\rangle|^2$ for these four eigen-states are in the form of Eq. (2).
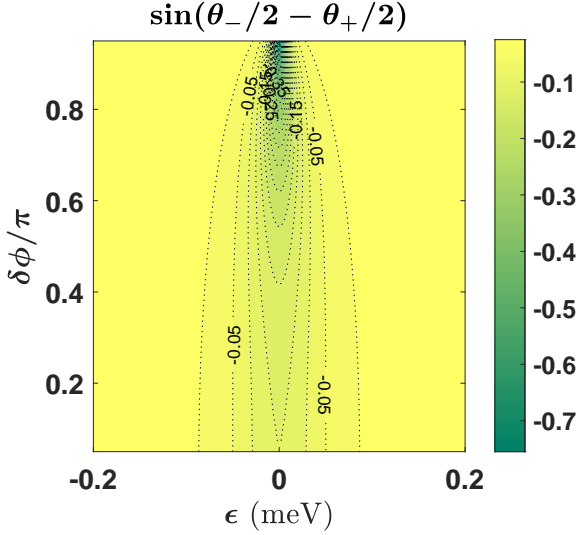
$$\sin(\theta_-/2 - \theta_+/2)$$

Figure 3. Accuracy of approximate diagonalization under different conditions. The valley splittings are $|\Delta_L| = 0.045$ meV, $|\Delta_R| = 0.055$ meV.

Accuracy of the approximate solution

The eigen-states (22-25) are obtained when $|\Delta_L| = |\Delta_R|$. Practically, $|\Delta_L|$ is usually not identical to $|\Delta_R|$. However the charge distributions in Eq. (2) remain a good approximation. This is because in most cases the nearby dots have similar valley splittings $|\Delta_L| \approx |\Delta_R|$, which makes $\sin\left(\frac{\theta_-}{2} - \frac{\theta_+}{2}\right) \approx 0$. As such, the term $\langle\psi_{1,-}|H_1|\psi_{1,+}\rangle$ that we neglected is generally a small correction compared to $\langle\psi_{1,-}|H_1|\psi_{2,+}\rangle$. Even if $|\Delta_L|$ and $|\Delta_R|$ is quite different, our numerical results in Fig. 3 suggest only a small error in Eq. (2).

In Fig. 3, we plot the factor $\sin\left(\frac{\theta_-}{2} - \frac{\theta_+}{2}\right)$ under different QD parameters. It shows that in most region, the factor we have neglected in Eq. (15) is quite small. Only in the very special case when the phase difference $\delta\phi \to \pi$ and the detuning $\epsilon \to 0$, the factor $\sin\left(\frac{\theta_-}{2} - \frac{\theta_+}{2}\right)$ is notable. Otherwise, Eq. (2) is always a good approximation. Besides, for any $\delta\phi$ and $|\Delta_{L,R}|$, the notable deviation always appears near $\epsilon = 0$. If we consider the average of $\sin\left(\frac{\theta_-}{2} - \frac{\theta_+}{2}\right)$ over all ϵ (because the fitting depends on the charge distribution over all ϵ, not just at $\epsilon = 0$), the average deviation is always small. For example, when there is a 20% difference between the two valley splittings, $|\Delta_-|/|\Delta_+| = 0.2$, the overall magnitude (average value over different ϵ) of the factor $\sin\left(\frac{\theta_-}{2} - \frac{\theta_+}{2}\right)$ is only 4% of the factor $\cos\left(\frac{\theta_-}{2} - \frac{\theta_+}{2}\right)$. Namely, the terms we dropped are indeed negligible even when there is a notable difference between the two valley splittings.

Details of data fitting

In the "Results" section, we show all the fitting results in Table I and the raw data of data set (c) in Fig. 1. Here, we show all the other 7 sets of raw data and the best fitting curves. The raw data are extracted from the readout of the QPC sensor directly and the best fitting curves are shown in Fig. 4. For panels (a), (b) and (d), the data are measured from QD 1-2, with different barrier gate voltage V_{B2} (which tunes t_C). The valley splitting $|\Delta_L|$ and $|\Delta_R|$ are not actually measured directly in the experiment, and are estimated to be around 66-74 μeV [57]. We perform the curve fitting with several groups of $|\Delta_L|$ and $|\Delta_R|$ ranging from 66-74 μeV, as shown in Fig. 5. The data presented in Tables I is picked because the fitting results of $\delta\phi$ are relatively consistent. We choose this criterion because the only tuned parameter in the experiment is t_C, which would generally not affect $\delta\phi$ when it is not varied too significantly. Interestingly, Fig. 5 shows that other estimates of $|\Delta_L|$ lead to very similar results on $\delta\phi$. The fitting results of $\delta\phi$ is always around 2.2 rad. The value of $\delta\phi$ fitted from data set (d) has a small difference from the results from other data sets (a), (b) and (c). We believe this is mostly because data set (d) has larger noise in the raw data of I_{QPC}, which is apparent in Fig. 4. In short, our fitting procedure does not seem to be overly sensitive to the choices of the valley splittings, as long as they are not too different across the two dots.

We highlight data set (d) in Fig. 4 because it has the largest t_C, making the difference between 2L fitting curve and 4L fitting curve clearly observable with bare eyes. One can easily see the 4L curve fits better to the raw data. The curve obtained by using Eq. (2) almost coincide with the curve obtained by fully numerical diagonalization, illustrating the robustness of our approximate expressions. Besides, we would also like to emphasize that the actual 2L and 4L fitting results for (d) are quite different (almost 100% according the results in Table I), much larger than it seems from the two curves.

Similarly, the best curve fittings of the data measured from QD 2-3 are shown in Fig. 4 (e)-(h). The most interesting result is the last panel (h). It is discussed that the 2L theory predicts $t_C(h)$ to be smaller than $t_C(g)$, while the 4L theory suggests that $t_C(h)$ is larger than $t_C(g)$. Experimentally, it is expected that the true value of t_C in panel (h) should be larger because the gate voltage V_{B3} used to tune t_C between dot 2-3 is increased from (g) to (h) when the experiment is performed. Here, Fig. 4 (h) shows this set of data is obviously measured with a notably larger noise than other sets. This large noise leads to more significant error for the fitting results. However, we also see that even with such a large noise the 4L fitting still make a prediction which does not contradict with the experimental setup.
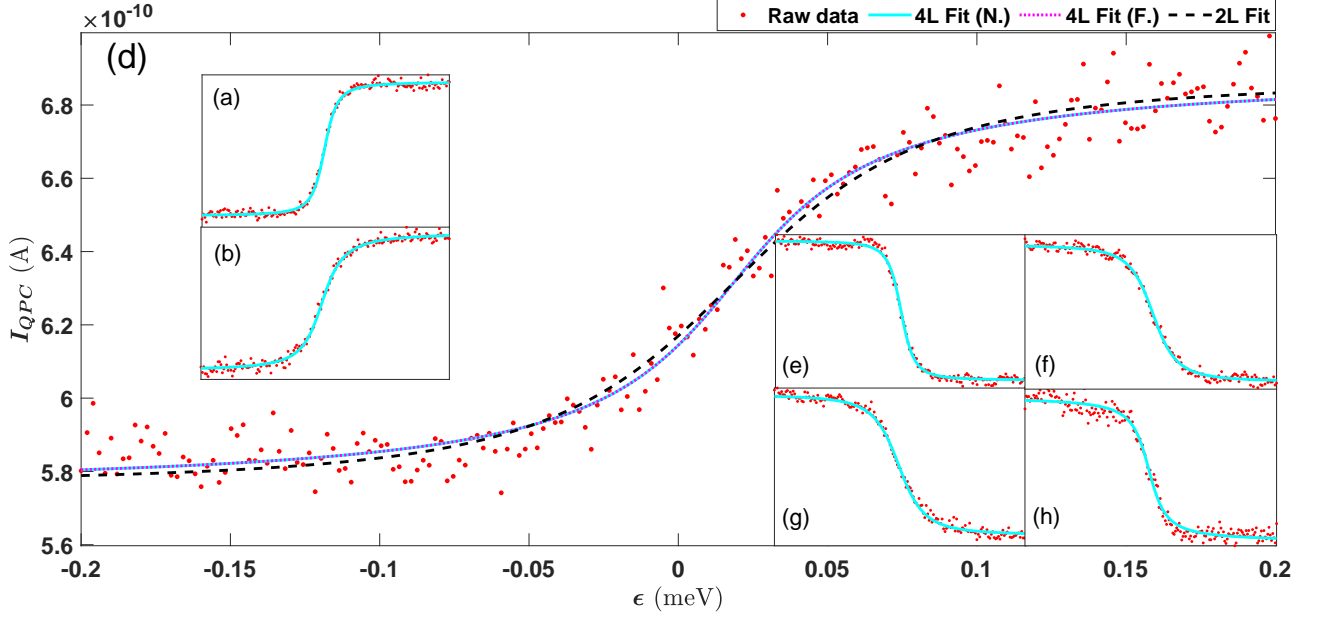
Figure 4. Curve fitting for actual data measured from experiment. (a), (b) and main plot (d) are obtained from the left two dots (dot 1 and 2) with different barrier gate voltage. (e)-(h) in the right-bottom corner are measured from right two dots (2 and 3). Data set (c) is absent since it is presented in Fig. 1.
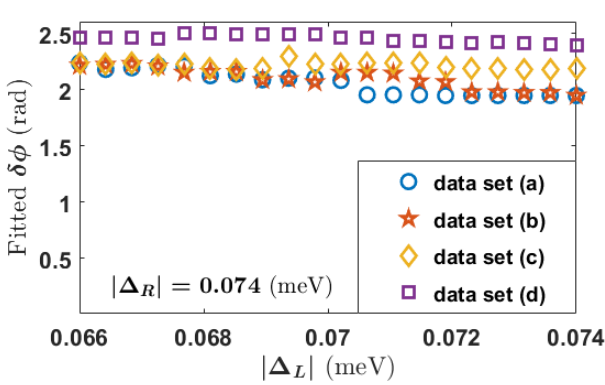

Figure 5. Fitting results of $\delta\phi$ by using various combination of $|\Delta_L|$ and $|\Delta_R|$.

Figure 6. Intuitive difference of two fitting formulas. Parameters are $t_C = 50\mu$eV, $|\Delta_L| = 74\mu$eV. $|\Delta_R|$ and $\delta\phi$ are given in each subplot. ϵ is ranging from -0.2 meV to 0.2 meV.

Difference between 2L and 4L fitting curves

The difference between the 2L fitting curve and the 4L fitting curve in Fig. 1 looks insignificant. This is mostly because the particular parameters in the experiment happen to produce similar 2L and 4L curves, even though the corresponding tunnel coupling strengths are quite different. In Fig. 6, we show that the differences between a 2L and a 4L fitting curves can both be minimal and be dramatic. For example, very different valley splittings $|\Delta_{L,R}|$ in the two dots makes the 4L curve lose its symmetry around zero detuning, while a 2L curve is always symmetric. The two fitting curve can also be easily distinguished when the condition (7) is not fulfilled.
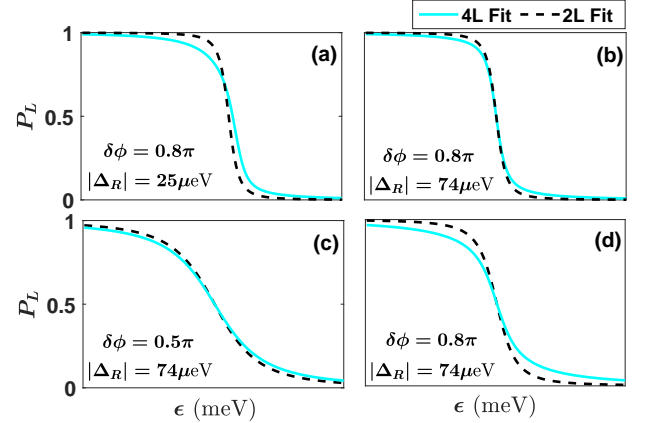
Even when two curves look very similar, they may yield very different fitting results. For instance, the curves in Fig. 4 (d) look quite similar, but there is nearly 90% difference between the 2L and 4L fitting results on $|t_+|$ in Table I.

Estimation of fitting parameters I_0, δI, and ϵ_0

In the "Results" section, we describe our fitting procedure by splitting the fitting parameters into two groups: (1) I_0, δI, and ϵ_0, which determine the position of the fit-
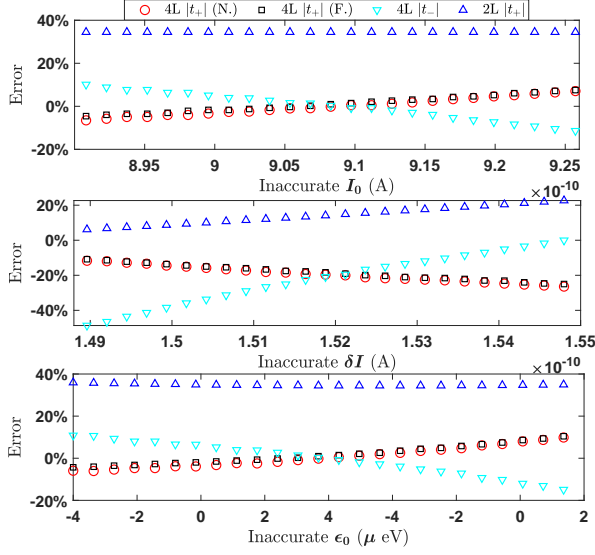
Figure 7. Fitting error caused by wrong estimation of I_0, δI, and ϵ_0. Parameters are the same as Table I, QD 1-2.

ting curve; and (2) t_+ and t_-, which determine the shape of the curve. In our protocol we fit the two groups of parameters in turn until the results converge. Practically, we only perform the iterative fitting 2 rounds because a bad estimate on I_0, δI, and ϵ_0 does not result in too much error on the final fitting results of $t_\pm$. In Fig. 7, we plot the fitting error caused by a wrong estimate of I_0, δI, and ϵ_0. Fig. 7 is plotted in a relative wide range. However, practically the errors cannot be too large, otherwise the best fitting curve will have a notable shift. Therefore, the iterative fitting converge very fast and 2 rounds of fitting is generally enough.

fitting error caused by incomplete knowledge of system parameters

Valley parameters such as $|\Delta_L|$, $|\Delta_R|$ are crucial in describing a Si DQD. As shown in Eq. (2) and (3), the fitting protocol in our model requires a preliminary measurement on the valley splitting of the two dots. Practically, the valley splittings may be unknown or only roughly estimated. In the example in Table I, the valley splittings are indeed estimated bu not measured. It is thus important to know the impact on the accuracy of $t_\pm$ by inexact knowledge of $|\Delta_{L,R}|$.

In Fig. 8 we plot the error caused by incomoplete knowledge of valley splitting $|\Delta_{L,R}|$. The numerical data used in fitting are generated with $|\Delta_{L,R}| = 74$ μeV. We then vary $|\Delta_L|$ or $|\Delta_R|$ on purpose to examine the sensitivity of our protocol to this systematic error.

The numerical results show that a moderately off estimate of $|\Delta_{L,R}|$ will not lead to sizable errors in 4L fitting unless $|\Delta_{L,R}|$ is significantly underestimated. In
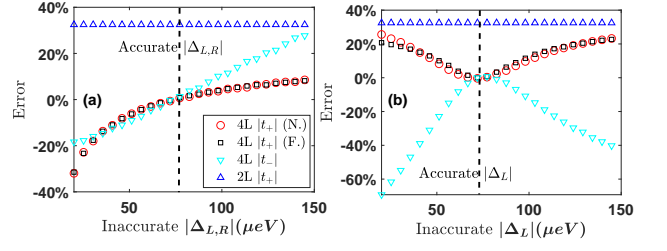

Figure 8. Fitting error by different methods, the "pseudo-curve" data is obtained with $t_C = 0.071$ meV, $|\Delta_L| = |\Delta_R| = 0.074$ meV, and $\delta\phi = 0.7\pi$. Inaccurate $|\Delta_{L,R}|$ indicate a wrong estimation/measurement on $|\Delta_{L,R}|$. In (a), we assume $|\Delta_L| = |\Delta_R|$. In (b), we assume $|\Delta_R|$ is measured accurately, only $|\Delta_L|$ has an error.

Fig. 8 (a), when $|\Delta_{L,R}| \approx 37$ μeV (50% underestimated), the 4L fitting error is still only about 10%. Furthermore, an overestimated $|\Delta_{L,R}|$ will result in even smaller error comparing to an underestimated $|\Delta_{L,R}|$, and the 4L fitting error is always smaller than the 2L fitting. The right panel (b) shows the case that only one valley splitting ($|\Delta_L|$) is known inaccurately. Similar to panel (a), the 4L fitting error is always smaller than the 2L fitting. We note that the fitting accuracy of inter-valley tunnel coupling $|t_-|$ is more sensitive to the knowledge of $|\Delta_L|$, though information on t_- is not accessible at all to a 2L model, since valley physics is not included there.

Another source of error in tunnel couplings is the measurement of the current I_{PQC}, which always contains some noise δI_{noise} as shown in Eq. (6) and illustrated in Fig. 1. Here, we use a stochastic function δI_{noise} to simulate the uncertainty in current measurement. The stochastic function is characterized by the mean $\langle \delta I_{noise} \rangle = 0$ and the standard deviation $\sigma(\delta I_{noise})$, which indicates the strength of the noise. Numerical results as presented in Table II show that the noise δI_{noise} has a much larger impact on the performance of 2L fitting comparing to the 4L fitting. By using the 4L model, even when the relative strength of the noise reaches 5%, the fitting error is still under 10%, while the 2L fitting always produces a significant error over 35%. The errors from 4L fitting do increase rapidly with an increasing $\sigma(\delta I_{noise})$, while errors in the 2L fitting remains large and do not change dramatically as $\sigma(\delta I_{noise})$ increases.

$\frac{\sigma(\delta I_{noise})}{\delta I}$	0.01	0.02	0.03	0.04	0.05
Error on $|t_+|$ (2L)	36.87%	36.53%	36.18%	36.82%	37.18%
Error on $|t_+|$ (4L)	1.56%	4.30%	4.98%	6.25%	8.19%
Error on $|t_-|$ (4L)	1.06%	2.81%	3.54%	4.16%	4.68%

Table II. Fitting error caused by noise on I_{QPC} measurement.

DATA AVAILABILITY

Data and an example of fitting code are available from the authors on reasonable request.

ACKNOWLEDGEMENTS

AUTHOR CONTRIBUTIONS

X.Z. and X.H. contributed to theoretical/numerical/physical analysis and prepared the manuscript.

ADDITIONAL INFORMATION

Competing Interests: The authors declare no competing interests.

[1] F. A. Zwanenburg, A. S. Dzurak, A. Morello, M. Y. Simmons, L. C. L. Hollenberg, G. Klimeck, S. Rogge, S. N. Coppersmith, and M. A. Eriksson, Rev. Mod. Phys. **85**, 961 (2013).

[2] R. Hanson, L. P. Kouwenhoven, J. R. Petta, S. Tarucha, and L. M. K. Vandersypen, Rev. Mod. Phys. **79**, 1217 (2007).

[3] M. Gullans and J. Petta, Physical Review B **102**, 155404 (2020).

[4] A. Mills, D. Zajac, M. Gullans, F. Schupp, T. Hazard, and J. Petta, Nature communications **10**, 1 (2019).

[5] J. Petta, H. Lu, and A. Gossard, Science **327**, 669 (2010).

[6] R. M. Otxoa, A. Chatterjee, S. N. Shevchenko, S. Barraud, F. Nori, and M. F. Gonzalez-Zalba, Physical Review B **100**, 205425 (2019).

[7] M. Kervinen, J. E. Ramírez-Muñoz, A. Välimaa, and M. A. Sillanpää, Physical review letters **123**, 240401 (2019).

[8] N. E. Penthorn, J. S. Schoenfield, J. D. Rooney, L. F. Edge, and H. Jiang, npj Quantum Information **5**, 1 (2019).

[9] B. Joecker, P. Cerfontaine, F. Haupt, L. R. Schreiber, B. E. Kardynał, and H. Bluhm, Physical Review B **99**, 205415 (2019).

[10] X. Zhang, H.-O. Li, G. Cao, M. Xiao, G.-C. Guo, and G.-P. Guo, National Science Review **6**, 32 (2019).

[11] E. Cota and S. E. Ulloa, Journal of Physics: Condensed Matter **30**, 295301 (2018).

[12] F. Martins, F. K. Malinowski, P. D. Nissen, S. Fallahi, G. C. Gardner, M. J. Manfra, C. M. Marcus, and F. Kuemmeth, Physical review letters **119**, 227701 (2017).

[13] J. S. Schoenfield, B. M. Freeman, and H. Jiang, Nat. Commun. **8**, 64 (2017).

[14] B.-B. Chen, B.-C. Wang, G. Cao, H.-O. Li, M. Xiao, G.-C. Guo, H.-W. Jiang, X. Hu, and G.-P. Guo, Physical Review B **95**, 035408 (2017).

[15] D. Culcer, X. Hu, and S. Das Sarma, Phys. Rev. B **82**, 205315 (2010).

[16] D. Culcer, Ł. Cywiński, Q. Li, X. Hu, and S. Das Sarma, Phys. Rev. B **82**, 155312 (2010).

[17] Q. Li, Ł. Cywiński, D. Culcer, X. Hu, and S. Das Sarma, Phys. Rev. B **81**, 085313 (2010).

[18] X. Li, E. Barnes, J. P. Kestner, and S. Das Sarma, Phys. Rev. A **96**, 012309 (2017).

[19] Z. Shi, C. Simmons, J. Prance, J. K. Gamble, T. S. Koh, Y.-P. Shim, X. Hu, D. Savage, M. Lagally, M. Eriksson, et al., Phys. Rev. Lett. **108**, 140503 (2012).

[20] T. S. Koh, J. K. Gamble, M. Friesen, M. Eriksson, and S. Coppersmith, Phys. Rev. Lett. **109**, 250503 (2012).

[21] D. Kim, Z. Shi, C. Simmons, D. Ward, J. Prance, T. S. Koh, J. K. Gamble, D. Savage, M. Lagally, M. Friesen, et al., Nature **511**, 70 (2014).

[22] G. Cao, H.-O. Li, G.-D. Yu, B.-C. Wang, B.-B. Chen, X.-X. Song, M. Xiao, G.-C. Guo, H.-W. Jiang, X. Hu, et al., Physical review letters **116**, 086801 (2016).

[23] E. Ferraro, M. De Michielis, G. Mazzeo, M. Fanciulli, and E. Prati, Quantum information processing **13**, 1155 (2014).

[24] J. Taylor, H.-A. Engel, W. Dür, A. Yacoby, C. Marcus, P. Zoller, and M. Lukin, Nat. Phys. **1**, 177 (2005).

[25] K. Takeda, A. Noiri, J. Yoneda, T. Nakajima, and S. Tarucha, Phys. Rev. Lett. **124**, 117701 (2020).

[26] F. Ginzel, A. R. Mills, J. R. Petta, and G. Burkard, Physical Review B **102**, 195418 (2020).

[27] B. Buonacorsi, B. Shaw, and J. Baugh, Physical Review B **102**, 125406 (2020).

[28] T. Fujita, T. A. Baart, C. Reichl, W. Wegscheider, and L. M. K. Vandersypen, npj. Quantum Information **3** (2017), 10.1038/s41534-017-0024-4.

[29] J. Villavicencio, I. Maldonado, E. Cota, and G. Platero, Physical Review B **88**, 245305 (2013).

[30] J. Zhang, L. Greenman, X. Deng, I. M. Hayes, and K. B. Whaley, Physical Review B **87**, 235324 (2013).

[31] X. Zhao, P. Huang, and X. Hu, Sci. Rep. **6**, 23169 (2016).

[32] X. Zhao and X. Hu, Sci. Rep. **8**, 13968 (2018).

[33] D. Zajac, T. Hazard, X. Mi, E. Nielsen, and J. Petta, Phys. Rev. Appl **6**, 054013 (2016).

[34] A. Tyryshkin, J. Morton, S. Benjamin, A. Ardavan, G. Briggs, J. Ager, and S. Lyon, J. Phys.: Condens. Matter **18**, S783 (2006).

[35] H. Bluhm, S. Foletti, I. Neder, M. Rudner, D. Mahalu, V. Umansky, and A. Yacoby, Nat. Phys. **7**, 109 (2011).

[36] K. D. Petersson, L. W. McFaul, M. D. Schroer, M. Jung, J. M. Taylor, A. A. Houck, and J. R. Petta, Nature **490**, 380 (2012).

[37] A. M. Tyryshkin, S. Tojo, J. J. Morton, H. Riemann, N. V. Abrosimov, P. Becker, H.-J. Pohl, T. Schenkel, M. L. Thewalt, K. M. Itoh, et al., Nat. Mater. **11**, 143 (2012).

[38] K. Saeedi, S. Simmons, J. Z. Salvail, P. Dluhy, H. Riemann, N. V. Abrosimov, P. Becker, H.-J. Pohl, J. J. L. Morton, and M. L. W. Thewalt, Science **342** (2013).

[39] M. Veldhorst, J. C. C. Hwang, C. H. Yang, A. W. Leenstra, B. de Ronde, J. P. Dehollain, J. T. Muhonen, F. E. Hudson, K. M. Itoh, A. Morello, and A. S. Dzurak, Nat. Nanotechnol. **9**, 981 (2014).

[40] A. J. Sigillito, R. M. Jock, A. M. Tyryshkin, J. W. Beeman, E. E. Haller, K. M. Itoh, and S. A. Lyon, Phys. Rev. Lett. **115**, 247601 (2015).

[41] L. DiCarlo, H. J. Lynch, A. C. Johnson, L. I. Childress, K. Crockett, C. M. Marcus, M. P. Hanson, and A. C. Gossard, Phys. Rev. Lett. **92**, 226801 (2004).

[42] S. Shevchenko, S. Ashhab, and F. Nori, Phys. Rep. **492**, 1 (2010).

[43] J. Petta, A. Johnson, C. Marcus, M. Hanson, and A. Gossard, Phys. Rev. Lett. **93**, 186802 (2004).

[44] J. J. Pla, K. Y. Tan, J. P. Dehollain, W. H. Lim, J. J. Morton, D. N. Jamieson, A. S. Dzurak, and A. Morello, Nature **489**, 541 (2012).

[45] H. Eenink, L. Petit, W. Lawrie, J. Clarke, L. Vandersypen, and M. Veldhorst, Nano letters **19**, 8653 (2019).

[46] A. Sigillito, J. Loy, D. Zajac, M. Gullans, L. Edge, and J. Petta, Phys. Rev. Applied **11**, 061006 (2019).

[47] A. Mills, M. Feldman, C. Monical, P. Lewis, K. Larson, A. Mounce, and J. R. Petta, Appl. Phys. Lett. **115**, 113501 (2019).

[48] C. Simmons, M. Thalakulam, B. Rosemeyer, B. Van Bael, E. Sackmann, D. Savage, M. Lagally, R. Joynt, M. Friesen, S. Coppersmith, *et al.*, Nano Lett. **9**, 3234 (2009).

[49] J. Yoneda, W. Huang, M. Feng, C. Yang, K. Chan, T. Tanttu, W. Gilbert, R. Leon, F. Hudson, K. Itoh, *et al.*, arXiv preprint arXiv:2008.04020 (2020).

[50] A. Jones, E. Pritchett, E. Chen, T. Keating, R. Andrews, J. Blumoff, L. De Lorenzo, K. Eng, S. Ha, A. Kiselev, *et al.*, Phys. Rev. Applied **12**, 014026 (2019).

[51] T. Ota, T. Hayashi, K. Muraki, and T. Fujisawa, Applied Physics Letters **96**, 032104 (2010).

[52] J. Stehlik, Y. Dovzhenko, J. R. Petta, J. Johansson, F. Nori, H. Lu, and A. Gossard, Physical Review B **86**, 121303 (2012).

[53] K. Petersson, C. Smith, D. Anderson, P. Atkinson, G. Jones, and D. Ritchie, Nano letters **10**, 2789 (2010).

[54] X. Mi, C. G. Péterfalvi, G. Burkard, and J. R. Petta, Phys. Rev. Lett. **119**, 176803 (2017).

[55] T. Ando, A. B. Fowler, and F. Stern, Rev. Mod. Phys. **54**, 437 (1982).

[56] C. Yang, A. Rossi, R. Ruskov, N. Lai, F. Mohiyaddin, S. Lee, C. Tahan, G. Klimeck, A. Morello, and A. Dzurak, Nat. Commun. **4**, 2069 (2013).

[57] A. Mills, private communication.

[58] B. Tariq and X. Hu, Phys. Rev. B **100**, 125309 (2019).